ORNL/SPR-2021/2397

Property data of irradiated SS 347 and irradiated, welded, and hydrogen charged Zircaloy-4 for the target solution vessel and support lines of SHINE

John Echols
Nathan Reid
Jordan Reed
Xiang (Frank) Chen
Chris Bryan
Lauren Garrison

March 2022

OAK RIDGE National Laboratory

ORNL IS MANAGED BY UT-BATTELLE LLC FOR THE US DEPARTMENT OF ENERGY

ORNL/SPR-2021/2397

Material Science and Technology Division

IRRADIATED STAINLESS STEEL 347 AND IRRADIATED, WELDED, AND HYDROGEN CHARGED ZIRCALOY-4 PROPERTY DATA FOR THE TARGET SOLUTION VESSEL AND SUPPORT LINES OF SHINE

John Echols
Nathan Reid
Jordan Reed
Xiang (Frank) Chen
Chris Brian
Lauren Garrison

March 2022

Prepared by
OAK RIDGE NATIONAL LABORATORY
Oak Ridge, TN 37831-6283
managed by
UT-BATTELLE LLC
for the
US DEPARTMENT OF ENERGY
under contract DE-AC05-00OR22725

ACKNOWLEDGMENTS
Support for this research was provided by the US Department of Energy's National Nuclear Security Administration (DOE/NNSA), Office of Material Management and Minimization, Molybdenum-99 Program. The authors would also like to thank the following coworkers for their contributions to completing this research project: Nesrin Cetiner, Doug Stringfield, Deborah Counce, and Eric Manneschmidt.

CONTENTS

ABSTRACT

In support of the reactor-vessel development effort of SHINE medical technologies, irradiation of its structural materials and post-irradiation testing have been performed in the High Flux Isotope Reactor at Oak Ridge National Laboratory. This irradiation was performed on welded and unwelded AISI 347 steel and Zircaloy-4 samples at low temperature (~60°C) in contact with the reactor coolant. Hardness, Charpy, and tensile data have been taken from all cases of unirradiated specimens, while post-irradiation tensile and hardness data have been taken from AISI 347 base metal and Zircaloy-4 base metal and weld specimens so far. Additionally, 3-point bend data have been taken from explosion-welded specimens. The expected changes to hardness, yield strength, ultimate tensile strength, uniform elongation, and total elongation as a result of the low temperature and low dose neutron irradiation are reported here.

1. INTRODUCTION

SHINE Medical Technologies will produce molybdenum-99 for medical isotope procedures by using a subcritical fusion-fission hybrid instrument [1]. Neutrons are produced by fusion and react with uranium in a uranyl sulfite solution, causing the nuclear reaction that leads to molybdenum-99 production for medical application. The target solution vessel (TSV) and all connecting welded piping will be exposed to neutron irradiation at low temperatures (below 100°C) and potential corrosion from the uranyl sulfite solution. Commonly used structural materials in light water fission reactors, including stainless steels and zircaloys, have a long history of successful service in a neutron environment. However, there is limited data or operating experience with these materials at the low temperatures of the TSV and piping. Especially, there is a need for data of low temperature irradiated welds of the candidate materials.

Zircaloy-4, AISI 347 stainless steel, and an AISI 347 layer clad on a low alloy carbon steel have been investigated for the TSV. Test plates of Zircaloy-4 and AISI 347 were welded to themselves using both gas tungsten arc welding (GTAW) and flux-cored arc welding (FCAW) because the vessel and pipes will have varying thicknesses that will require these different weld techniques. Select Zircaloy-4 samples were hydrogen charged to simulate potential hydrogen uptake from the solution in the TSV and to investigate the embrittlement hydrides can cause in zirconium alloys. These materials were irradiated in the High Flux Isotope Reactor (HFIR) at Oak Ridge National Laboratory (ORNL) to two fluences at approximately 60 °C. Testing has focused on the post-irradiation microhardness and tensile behavior of the Zircaloy-4 with and without hydrogen charging and on the AISI 347 base metal. The welded AISI 347 has been irradiated and mechanical property tests on the weld will be completed next.

2. EXPERIMENTAL METHODS

This section summarizes the supplier and composition information for the materials investigated, as well as gives an overview of the irradiation conditions and mechanical testing procedures. For additional details, especially on the material composition, unirradiated microstructure, and welding procedures please refer to previous reports [2,3].

2.1 MATERIAL INFORMATION

2.1.1 AISI 347

Three suppliers were used for the AISI 347: Penn Stainless, Rolled Alloys, and Sandmeyer Steel Company, so they could be compared. The elemental analysis conducted previously showed that all meet the ASTM A240 standard for chemical composition (as expected), but there was a notable difference in

their Mo impurity levels with Penn Stainless 0.029 weight percentage (wt.%), Sandmeyer 0.15 wt.%, and Rolled Alloys 0.3 wt% [3]. Since the isotope molybdenum-99 is the product of the SHINE system, Mo impurity in the TSV is undesirable. The Rolled Alloys and Penn Stainless materials had test sections welded with FCAW and GTAW by Vacuum Technology Inc., following a weld tracking procedure developed at ORNL using American Welding Society standards. More information about the elemental analysis, microstructure, and welding details of the three versions of AISI 347 can be found in [3].

The AISI 347 from each of the three suppliers had specimens cut from two directions perpendicular to each other, as shown in Figure 1. The direction of rolling of AISI 347 plates was not indicated by the manufacturers, and so the two directions are arbitrarily indicated as A and B for a total of six specimen varieties of the base metal. Crystallographic texture and microstructure analysis concluded that the direction A is the rolling direction for Penn stainless plate. The analysis showed the other two suppliers' materials had a mixture of multiple texture components and the rolling direction could not be conclusively determined, so the labeling convention A and B is maintained throughout these reports.

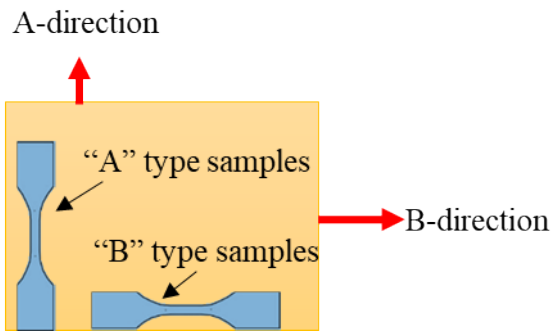

Figure 1. Tensile samples were cut in perpendicular directions (dubbed "A" and "B") from the parent 347 materials. EBSD was performed on the top surface of the parent material and can be seen in [2]. This figure is also reproduced from [2].

2.1.2 Explosion Welded Plate

A stainless chromium-nickel steel clad plate was manufactured and supplied by NobelClad. The clad plate has two layers that consist of a one-millimeter thick AISI 347 stainless steel flyer plate that was explosion welded to a 2 in thick SA-516-70 normalized carbon steel parent plate. The weld interface is a sinusoid with an amplitude of 0.17 mm. The center of the sinusoid interface is located at a depth of 0.96 mm below the surface of the stainless steel. The stainless steel layer has an austenitic microstructure. The carbon steel consists of a two-phase composite structure of ferrite and pearlite. The explosion weld interface has regions of plastic deformation and molten material. Information about the microstructure can be found in [3].

2.1.3 Zircaloy-4

The Zry-4 used in this work has a composition of Zr(bal.), 1.54 Sn, 0.21 Fe, and 0.11 Cr by percent weight, as reported by the manufacturer, ATI Specialty Alloys and Components. The material has been hot rolled, annealed, blasted, and pickled by the suppler. In order to understand the mechanical properties of Zry-4 welds in conditions they would experience in the TSV, the weld state, post-weld heat treatment (PWHT), irradiation condition, and hydrogen content were the four variables evaluated in this work. Table 1 summarizes the ranges of these variables.

Table 1. Summary of variables for Zry-4 materials. Each variable is represented by its column. For specific hydrogen charging values, see table 3 of [3].

Weld	**Post-weld heat treatment**	**Hydrogen (PPM)**	**Irradiation** E>0.1 MeV
None (Base metal)	None	None	None
GTAW	As welded	140-270	10^{20}n/cm^2
	600°C/1 hr PWHT	340-510	10^{21}n/cm^2

Unwelded material consists of small, equiaxed grains with an average grain size of 16µm when measured with circular intercept methods on micrographs. Following welding, fusion zones and heat affected zones form, each with their distinct microstructures. A representative image of the microstructure in a welded tensile bar is shown in Figure 2. A PWHT of 1 hour at 600°C was selected to remove residual stresses, following extensive optimization testing in previous years [3,4]. This PWHT shows significant recovery of ductility, while avoiding the formation of an undesirable "blocky alpha" microstructure [5] in the heat-affected zone of the welds and staying well below the beta-transition temperature near 900°C. Although higher temperature PWHTs (650-800°C) result in better ductility, this specific temperature was chosen out of an abundance of caution for concerns about precipitate coarsening at higher temperatures, which could affect corrosion properties. Additionally, a lower temperature is more achievable for PWHT of a large component such as the TSV. The microstructure of welded bars with and without PWHT has been documented extensively in previous reports [2,3].

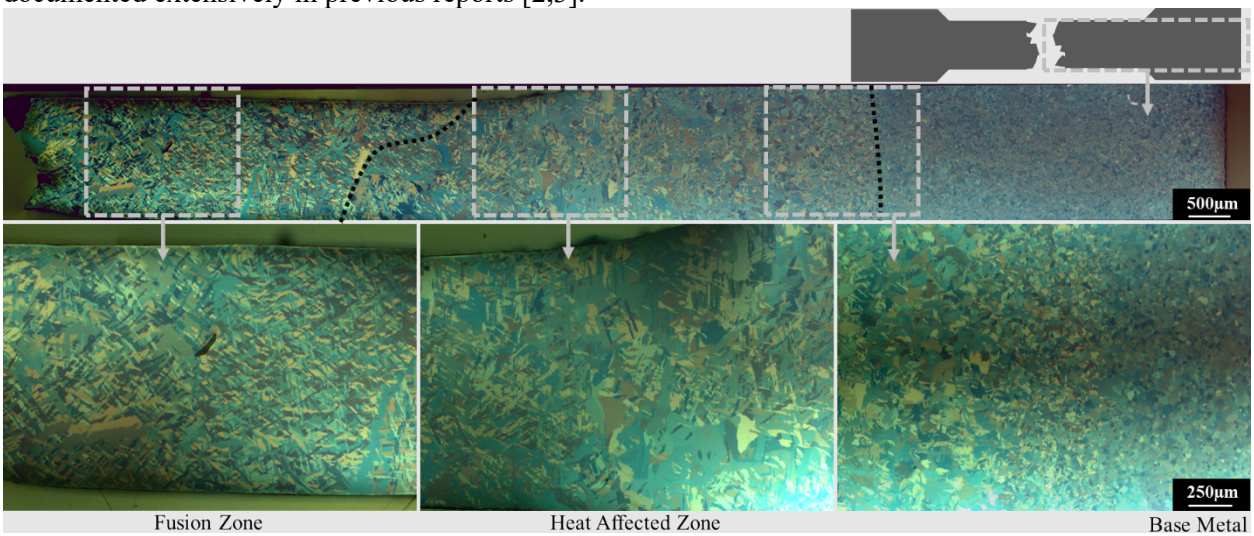

Figure 2. Polarized light composite micrograph, showing the microstructure of an unirradiated tensile bar (ZFD09) which underwent PWHT at 750 °C for 1hr as part of the PWHT optimization process. Gray boxes with arrows in the middle row indicate the area shown in the image on the bottom row. Black lines represent approximate boundaries between the fusion zone/HAZ (left) and the HAZ/base metal (right). Figure reproduced from [4] – see publication for a full discussion.

2.2 IRRADIATION

The materials were irradiated in two groups and both groups finished irradiation in FY21. The materials in group 1, from the rabbit capsules SHINE 11, 12, 13, and 14, were microhardness and tensile tested. The materials in group 2, rabbit capsules SHINE 15, 16, 17, and 18, were transported to the hot cells at ORNL and will be tested in the next FY. All capsules used the perforated capsule design, which has numerous holes in the capsule wall so that the samples can be in contact with the HFIR cooling water during irradiation, which is maintained at 60 °C. It is known that the sample temperature would be very slightly higher than 60 °C because of the energy deposited by the neutron irradiation in the materials and the gamma-heating as the samples become activated during irradiation. However, temperature measurement is not available or necessary for the perforated capsules, so a best estimate of the sample

irradiation temperatures is taken to be 60 °C. The irradiation used the hydraulic tube to achieve low fluences that are less than a full cycle of HFIR operation, which is typically about 25 days. Capsules SHINE 11 and 13 were irradiated for 32 hours; capsules SHINE 12 and 14 were irradiated for 366 hours. Each capsule was at a slightly different vertical position in HFIR, so the accumulated fluences for these times of irradiation were SHINE 11: $1.28*10^{20}$, SHINE 12: $1.29*10^{21}$, SHINE 13: $1.29*10^{20}$, and SHINE 14: $1.32*10^{21}$ n/cm^{21}(E>0.1 MeV).

2.3 MECHANICAL TESTING METHODS

2.3.1 Microhardness

Vickers microhardness testing on unirradiated samples was performed with a Future-Tech Corp. FM-700 digital microhardness tester for the base metal indents and a Wilson VH3100 microhardness tester with Buehler DiaMet software for the programmed lines of indentations. The hardness tests on irradiated samples were performed in Cell 4 of the 3025E hot cells at ORNL. Indent parameters for all samples were 0.5 kg force with 10 s dwell time. Indents had at least 3 indent widths of space between each indent or the edge of the sample. All irradiated samples tested were in the SS3 tensile type geometry. Unwelded specimens had 5 valid indents taken on each tensile tab for a total of 10 indents per sample. Welded specimens (ZNs and ZOs) had 2 lines of indents taken at spacings of roughly 0.5 mm along the tensile axis of the samples (see Figure 3). The fusion zone of the weld is in the gauge section, so this hardness indent pattern captures the base metal, left heat affected zone, fusion zone, right heat affected zone, and base metal from end to end of the tensile bar (Figure 3). Materials from the four irradiated capsules were tested (Table 2).

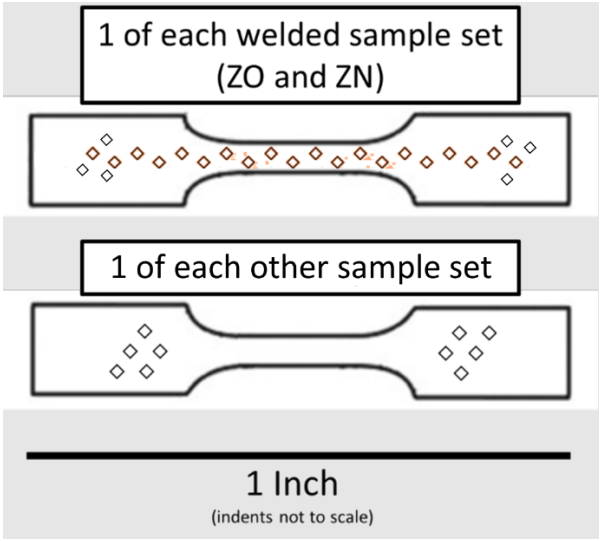

Figure 3. Illustration of microhardness indent pattern for the (top) welded samples and (bottom) base metal samples.

*Table 2. Irradiated samples were tested with microhardness and tensile. Two duplicate samples of each type were irradiated so are listed in the same row. R=Rolled Alloys; S=Sandmeyer Steel; P=Penn Stainless; BM=base metal; W=welded; WP=welded and post weld heat treated with 5 h ramp and 1 h hold at 600°C; *=samples that were microhardness tested in a row along the full length of the sample, all other samples were hardness tested only in the tensile tab regions.*

Capsule ID	Fluence (n/cm^2)	Sample ID	Sample ID	Material Type
SHINE 11	1.28E+20	Z-17	Z-20	Zry-4 BM; 220-230 ppm H
SHINE 11	1.28E+20	Z1-19	Z1-21	Zry-4 BM
SHINE 11	1.28E+20	ZO-33	ZO-34	Zry-4 W
SHINE 11	1.28E+20	ZN-33	ZN-34	Zry-4 WP
SHINE 12	1.29E+21	Z-18	Z-49	Zry-4 BM; 220-230 ppm H
SHINE 12	1.29E+21	Z1-17	Z1-18	Zry-4 BM
SHINE 12	1.29E+21	ZO-35	ZO-36*	Zry-4 W
SHINE 12	1.29E+21	ZN-37*	ZN-38	Zry-4 WP
SHINE 13	1.29E+20	RA-12	RA-13	R AISI 347 BM; a direction
SHINE 13	1.29E+20	SA-05	SA-11	S AISI 347 BM; a direction
SHINE 13	1.29E+20	PA-04	PA-06	P AISI 347 BM; a direction
SHINE 13	1.29E+20	PB-04	PB-06	P AISI 347 BM; b direction
SHINE 14	1.32E+21	RA-09	RA-11	R AISI 347 BM; a direction
SHINE 14	1.32E+21	SA-07	SA-08	S AISI 347 BM; a direction
SHINE 14	1.32E+21	PA-07	PA-08	P AISI 347 BM; a direction
SHINE 14	1.32E+21	PB-07	PB-08	P AISI 347 BM; b direction

2.3.2 Tensile Tests

The companion unirradiated samples were tested previously, with details provided in [3]. The irradiated samples listed in Table 2, except for those two marked with a *, were all tensile tested at room temperature after microhardness testing. The cell 1 Instron frame was used with a 5 kN load cell and an extension rate of 0.0003 in/s (0.00762 mm/s) and an acquisition rate of 10Hz. The tensile load and extension were recorded and used to calculate the stress and strain. A strain gauge was not used, so instead the approximate machine compliance was removed during the data analysis using the same method as used previously on this project and explained in further detail in [6]. This method results in accurate stress and strain values but does not produce an accurate Young's Modulus. When the data was plotted after this analysis, the initial elastic region was replaced with a vertical line. This method is appropriate because for these irradiation conditions, we expect little to no change in the elastic properties and the stress and total elongation values are most important for the application.

2.3.3 Charpy Impact Tests

Unirradiated Charpy testing of the AISI 347 steel from each of the suppliers was carried out on full-size Charpy specimens as illustrated in Figure 4. These tests were performed on an Instron Charpy frame at room temperature (22°C). Mini-size Charpy specimens with dimensions of 4.83 mm x 4.83 mm x 24.13 mm were cut from both the base metal and the welded AISI 347 plates. Part of the future work is to test the mini-size AISI 347 from each of the suppliers to validate the full-size to mini-size tests. Additionally, tests will be completed up to 100°C to capture the engineering properties of these austenitic steels in operational temperatures.

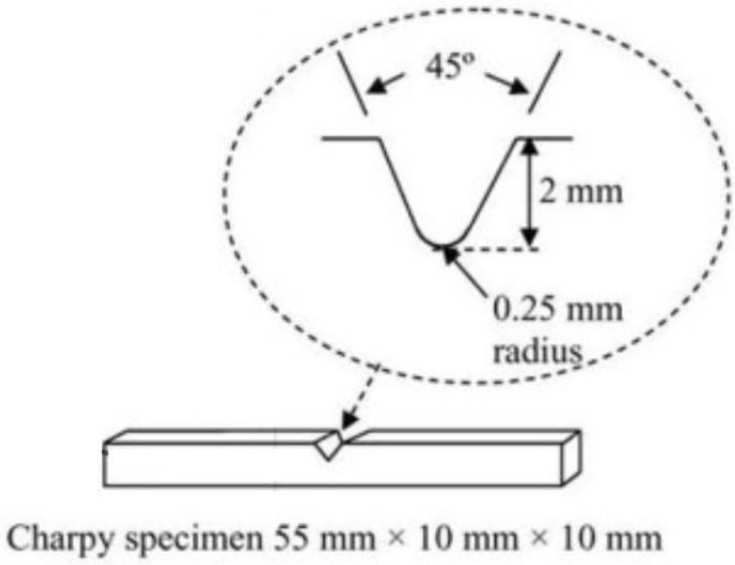

Figure 4 Schematic of the full-size Charpy specimens.

2.3.4 Miniature Disk Three-point Bend Tests

Three-point bending is a simple loading procedure to evaluate the bend stresses in the material and evaluate irradiation induced embrittlement. This test was done on disk specimens of 3 mm diameter and thicknesses ranging from 0.30 mm to 0.50 mm. Disks of this geometry are frequently used for small-size specimen testing after irradiation in HFIR. The loading and stress states in the specimen for a disk are shown in Figure 5. A load (P) is applied to the center of the disk with a diameter (D) in mm. The disk is supported on two ends which give a normal force response to the load. The supports are separated by a span length (L). The stresses that develop depend on the cross-sectional area of the disk, which depends on the thickness (h) and varying width (b(x)).

The fixture is a custom design made from 17-4 PH steel. The disk specimen makes contact with two support tungsten carbide rods with a 0.25 mm radius of curvature and one rod from which the load is applied. The span between supports is fixed at a distance of 2 mm. Bend stress and strain are calculated from the measured load and displacement using a simple beam bending equation that was modified for the geometry of the disk. For more details on the disk three-point bend for irradiated specimen testing, see [7].

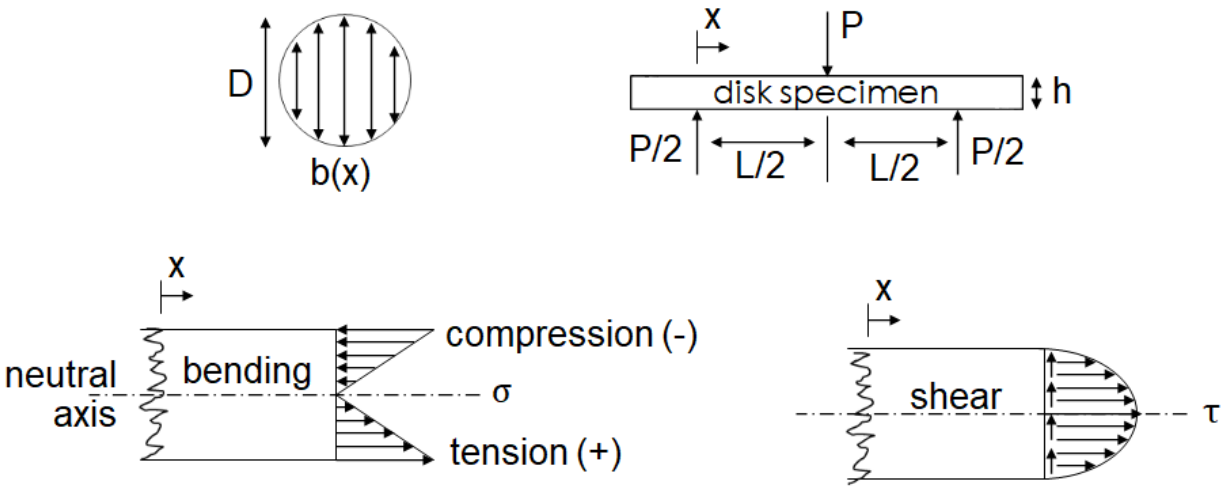

Figure 5. Schematic of the stresses in a disk specimen. The point of interest is in the maximum tension stress at break on the bottom surface of the disk, while minimizing shear stress by using smaller thickness h. Modified from [7]

2.3.5 Hot Cells

Irradiated specimens were evaluated in the Irradiation Material Evaluation and Testing (IMET) facility - a category III nuclear facility with six interconnected cells that has additional space in the cell access area for specimen prep and storage. This facility offers a variety of processing, testing, and imaging as well as maintains low enough levels to allow for human entrance into the cells for machine maintenance. Since most machines are the same as can be found in normal lab settings, specially designed fixtures are created to allow manipulator grips to load and operate machines (Figure 6).

Figure 6. (Left) Tensile bar holder used for SS3 specimens. (Right) Selection of tools with manipulator fittings to be used in IMET.

Two such specialized fixtures that were created for this project are a hardness stage and an SEM block, as seen in Figure 7. Both designs were made to 1) speed up the loading of specimens by the manipulator and 2) increase the reliability of specimen positioning. Previously, hardness tests were performed on a solid block flat surface, similar in shape to the current fixture but without the grooves or numbering. Without these grooves it was difficult to precisely align samples on the hardness tester stage and ensure they remained aligned during hardness mapping efforts. Additionally, without the grooves specimen could shift or slide off during loading attempts, which meant multiple loading attempts were sometimes required before testing could begin. For this project, the new fixture allowed for easier loading and alignment of samples to accomplish the two lines of indents following the tensile axis through the gauge

of the samples. In the past, to view fracture surfaces in the SEM, specimens were balanced vertically on carbon tape. This method was often quite time consuming and required several loading attempts or removing the stage from the SEM to adjust the sample if it fell over during imaging. To correct these issues the new SEM block has three slots for SS3 tensile sample halves held vertically and fits within the previous specimen holder.

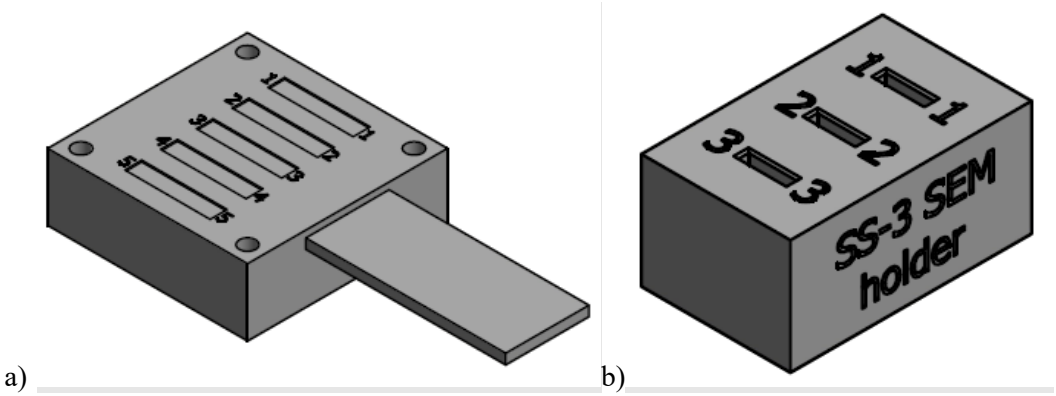

a) b)

Figure 7. Drawings of a) the SS3 hardness fixture, b) the SS3 SEM holder

3. RESULTS

3.1 AISI 347 ALLOY

Mechanical testing on the AISI 347 steels from the three suppliers was performed before and after irradiation in HFIR. Hardness and tensile testing were done at room temperature (22°C) for the unirradiated material and after neutron irradiation to ~10^{20} and 10^{21} n/cm^2 (E>0.1 MeV) (Table 2). Full-size Charpy specimens were tested at room temperature for the unirradiated case.

3.1.1 Hardness Tests

Microhardness testing using Vickers hardness tester was performed at a 0.5 kg load and 10 s dwell time on Penn, Rolled, and Sandmeyer AISI 347 stainless-steels. Hardness was taken for two directions of cuts on the Penn steel. The plots in Figure 9 show that the hardness value has a stark increase at the lower fluence neutron irradiation compared to the unirradiated case. An order of magnitude increase in neutron fluence resulted in some additional irradiation-induced hardening for all specimens, with the greatest increase in the Sandmeyer steel.

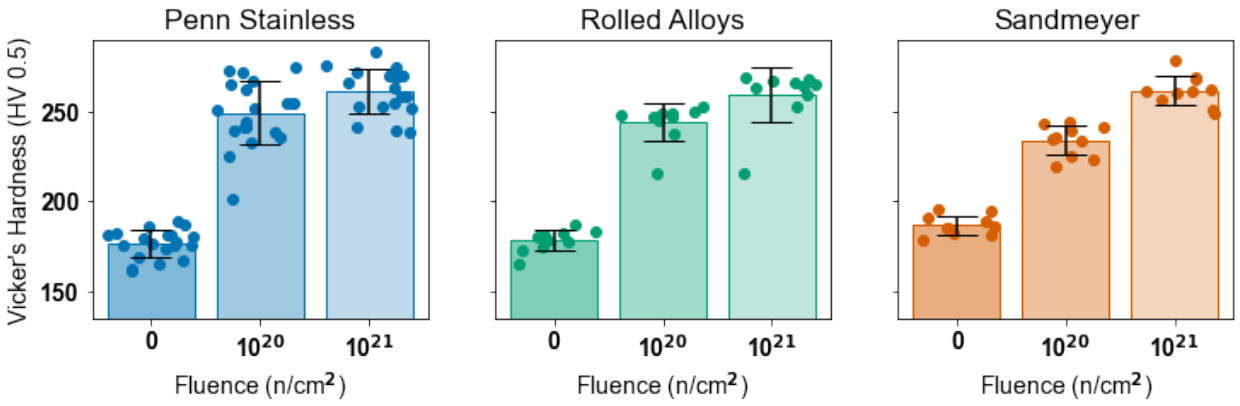

Figure 8. Hardness values for AISI 347 specimens. Dots represent individual data points, bars represent averages, and error bars represent one standard deviation. Fluences are E > 0.1 MeV.

3.1.2 Tensile Properties

Tensile curves were obtained from two directions of cuts on the Penn steel and one direction for the Rolled and Sandmeyer steels. Direction A is the rolling direction for Penn stainless plate, and direction B is perpendicular to the rolling direction (see Figure 1). For Rolled Alloys and Sandmeyer Steel, there was not a clear rolling direction identified in the crystallographic analysis, and they had less significant differences between the A and B direction unirradiated tensile tests as compared to Penn [3] so only one type of sample was irradiated. Two tensile tests were performed for each irradiation condition and additional tests were performed on the unirradiated materials. In Figure 10, the yield stress was calculated from the measured tensile curves at a 0.2 % strain offset. Ultimate stress was determined at the point of maximum stress. Lastly, the total elongation of the material was determined in strain percentage. The tensile curves are shown in Figure 11. Strengthening of the neutron irradiated steels is manifested in the form of a three-fold increase in yield strength followed by embrittlement by virtue of a loss of ductility shown by the large decrease in uniform elongation (hence, total elongation) and a smaller strain hardening region of the curve. The Rolled Alloy was the only steel to not have additional ductility loss at higher neutron fluences. Another feature of the higher fluence neutron irradiation is the appearance of an upper yield point in all the steels.

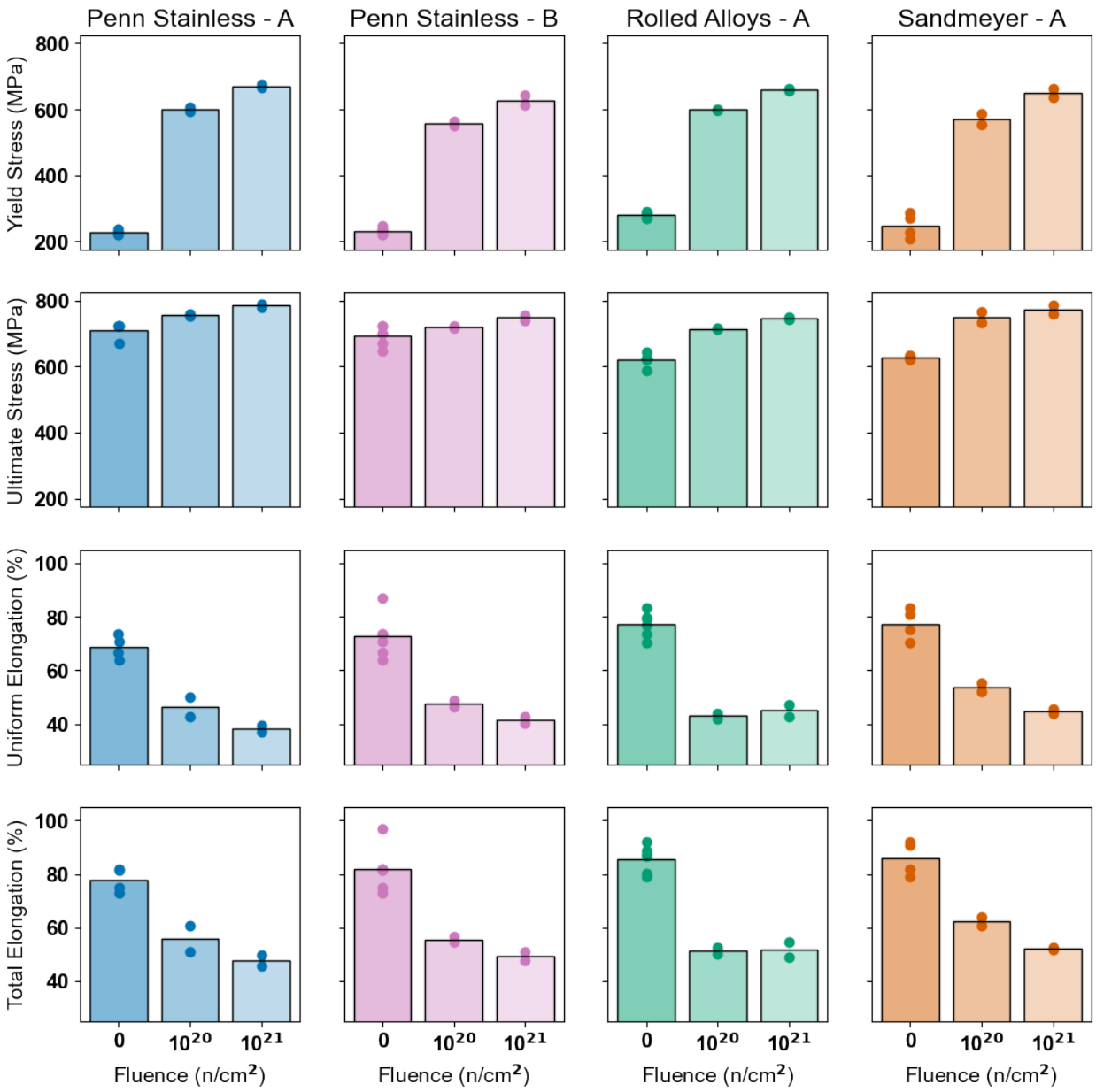

Figure 9. Tensile properties for AISI 347 specimens. Penn Stainless A is the rolling direction, and B is perpendicular to that. Rolled Alloys A and Sandmeyer A directions do not correspond to the rolling direction. Bars represent average values, while dots represent points from individual specimens. Fluences are for neutrons with E > 0.1 MeV.

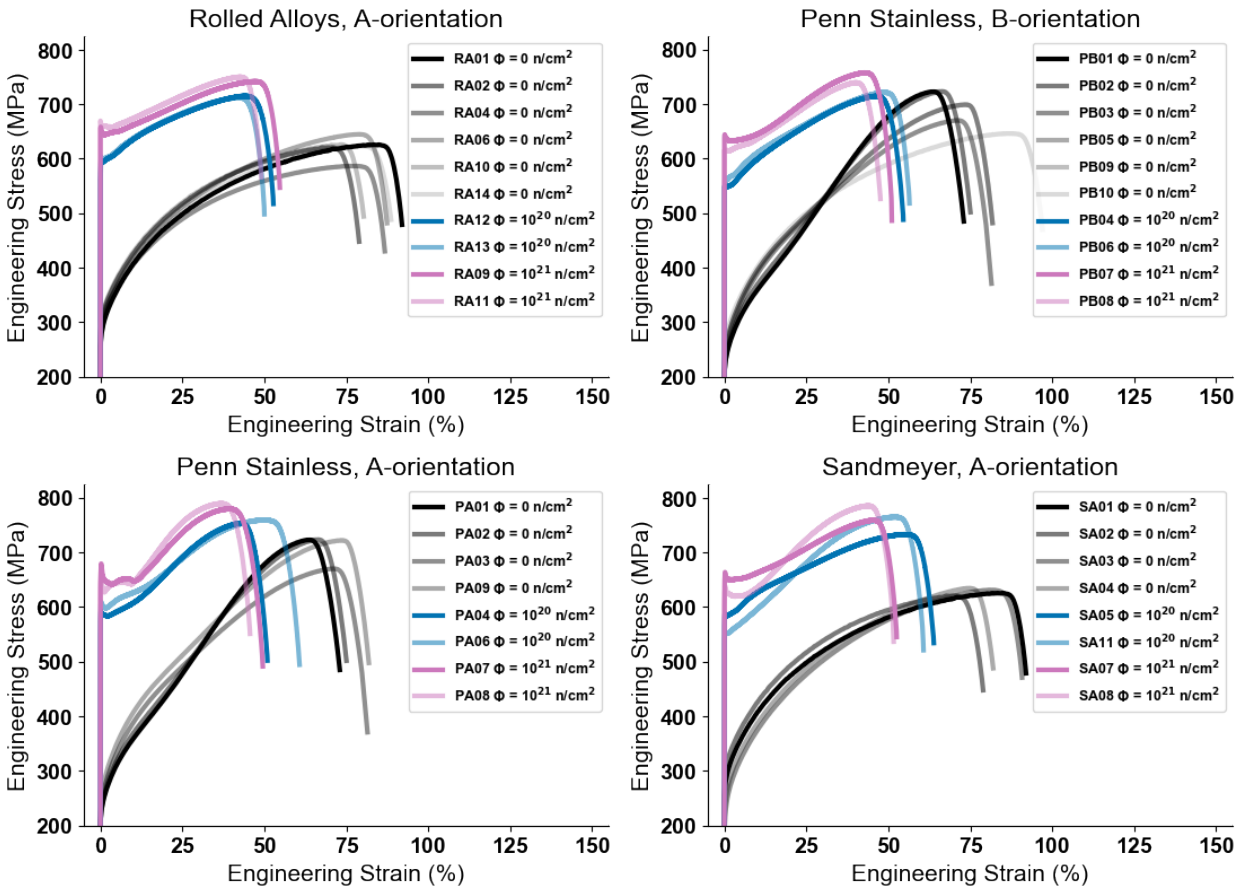

Figure 10. Tensile curves for tested AISI 347 specimens after analysis described in the Methods section. Penn Stainless A is the rolling direction, and B is perpendicular to that. Rolled Alloys A and Sandmeyer A directions do not correspond to the rolling direction.

3.1.3 Charpy Impact Testing

The room temperature impact properties of the AISI 347 steels from each supplier were determined by Charpy impact testing. The test was performed on five V-notch specimens for each material and the dial energy in Joules was recorded as shown in Figure 12. The Penn steel had the greatest absorbed energy and did not show any significant change with how the specimen was cut relative to the raw material orientation. This is notable because the tensile properties for Penn Stainless did show differences between the A (rolling) and B (perpendicular to rolling) directions. The direction of the specimen had a much stronger effect on the Charpy results of Rolled Alloys steel and a lesser effect on the Sandmeyer steel. In contrast, Rolled Alloys had the least differences between A and B direction unirradiated tensile properties and Sandmeyer had slight variation in tensile properties. None of the three had major grain sizes between the A and B directions, but in the Rolled Alloys steel had slightly more of a grain size difference than Penn or Sandmeyer.. See Figure 20 of [2] for a more detailed discussion of this microstructure.

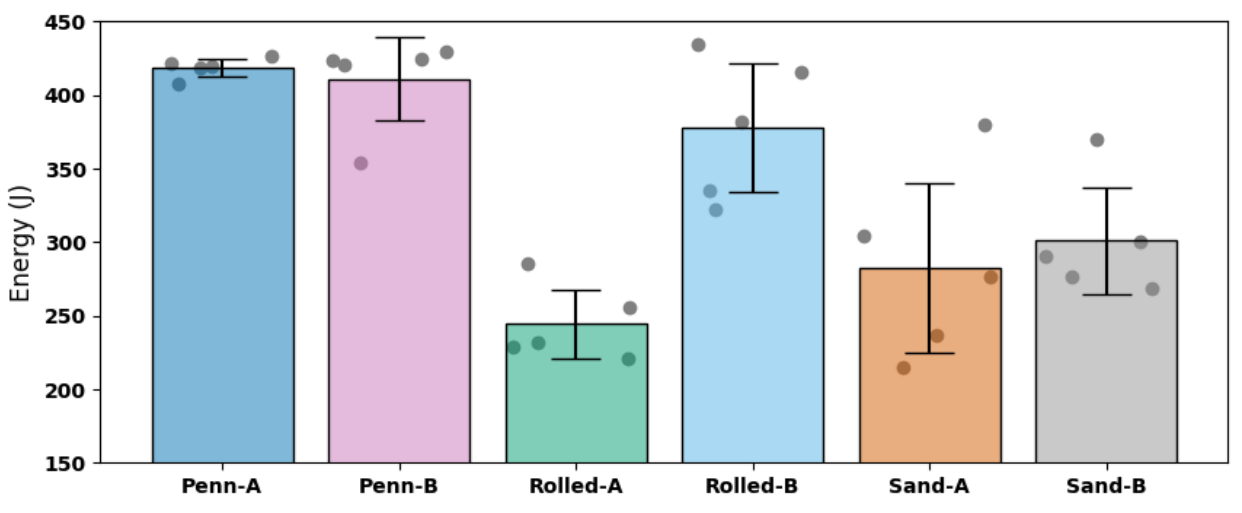

Figure 11. Charpy impact energy for unirradiated base metals.

3.2 EXPLOSION WELDED PLATE

A 1 mm thick AISI 347 stainless steel flyer plate was explosion welded to a 2 in thick SA-516-70 normalized carbon steel parent plate. A baseline uniaxial tensile strength was determined in [3]. Additional methods to determine the interface strength were also reported. The tensile strength of the interface region was determined with the tension force parallel to the interface. In this report, the microstructure of the two plates and the near-interface region were analyzed to relate microstructure to tensile and bend stress results.

3.2.1 Microstructure

The stainless-steel cladding has a deformed microstructure in the center and recrystallized regions within 20 µm of the interface. The carbon steel has large bulk grains of ferrite and pearlite with greater than 10 µm grain size. In Figure 12, the austenite microstructure has distinct boundaries where the explosion weld process creates severe plastic deformation and molten material as the interface is approached. In the deformed region, austenite grains are bimodal and have small and large grains intermixed as seen in Figure 13. The carbon steel parent plate has grain sizes greatly reduced in the plastic region. In the molten material region, the pearlite grains remain deformed and are highly elongated. The ferrite grains recrystallized and are larger.

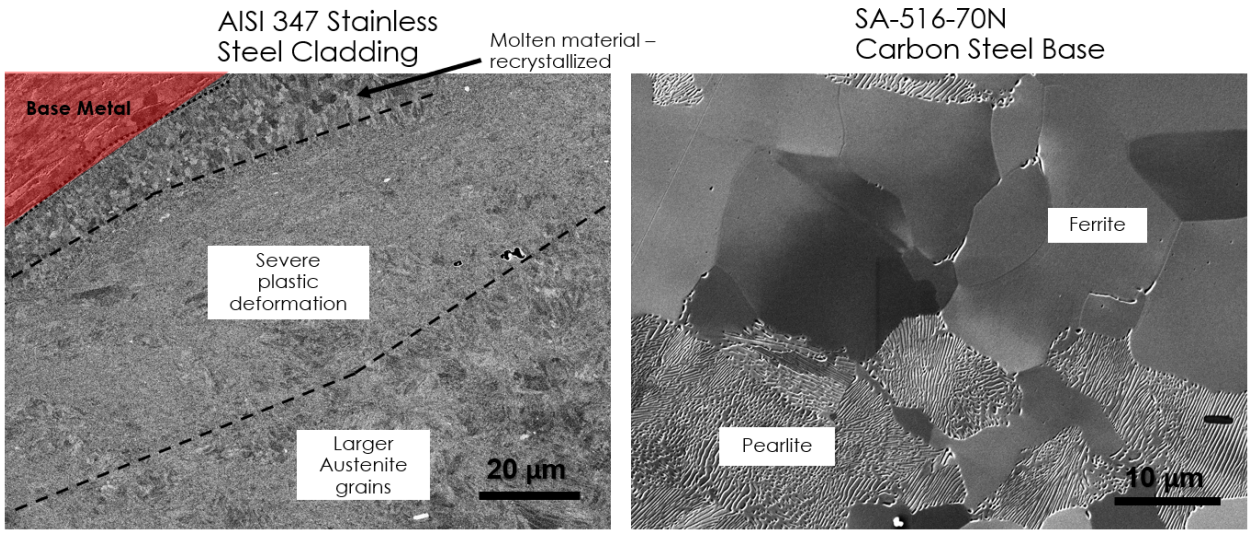

Figure 12. SEM micrographs of the explosion welded plate in regions further from the interface, showing bulk microstructure and changing microstructure as the interface is approached.

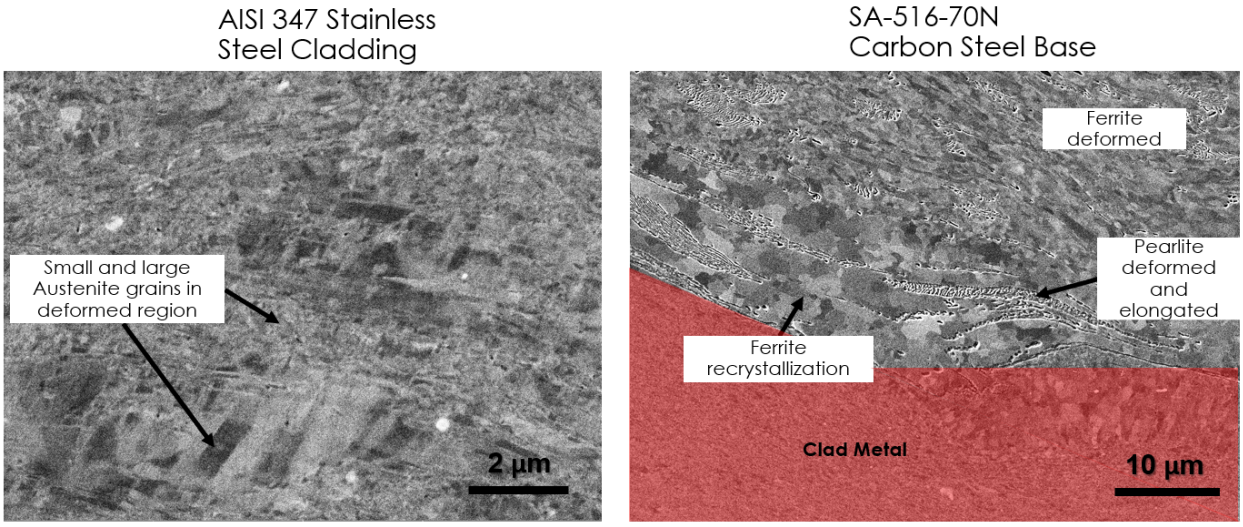

Figure 13. SEM micrographs of the explosion welded plate in regions near the interface. The near-interface has regions of deformed, elongated, and recrystallized grains due to the temperature and pressure of the explosion weld process.

3.2.2 Tensile Properties

Tensile curves of the AISI 347 stainless steel cladding, carbon steel base, and a bi-layer composite capturing the interface region are shown in Figure 14. The deformed microstructure near the interface results in increased strength in the tensile curves, with the strength primarily being carried by the stainless cladding material. As a result, the interface region has a reduced total elongation. Each constituent metal by themselves have roughly the same amount of ductility but differing strengths. From these curves, it was determined that there was no attrition of the tensile strength parallel to the interface due to explosive bonding. From the fracture surfaces in Figure 15, we see that the stainless component of the interface specimens contributes to the strength of the material and are the last regions to deform and fracture. The carbon-steel regions have a porous fracture surface and have a more sloped surface due to weaker strength and a higher amount of elongation in necking.

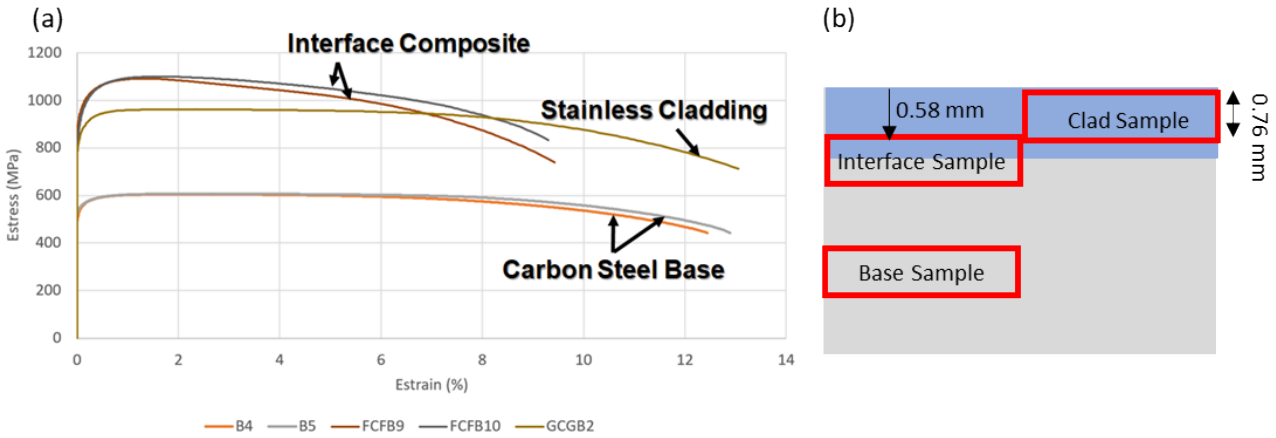

Figure 14. (a) Tensile curves (previously reported in [3]) (b) a diagram of the cross-section of the bulk plate from which specimens were cut. The SS3 type tensile samples are 0.76 mm thick, so the stainless cladding samples are entirely composed of the cladding material. The Interface Composite samples were cut 0.58 mm from the top of the material so that the clad to base interface would be approximately at their center, although in the real material the interface is a sinusoidal shape rather than flat. The Carbon Steel Base samples were cut entirely in the base metal region of the plate.

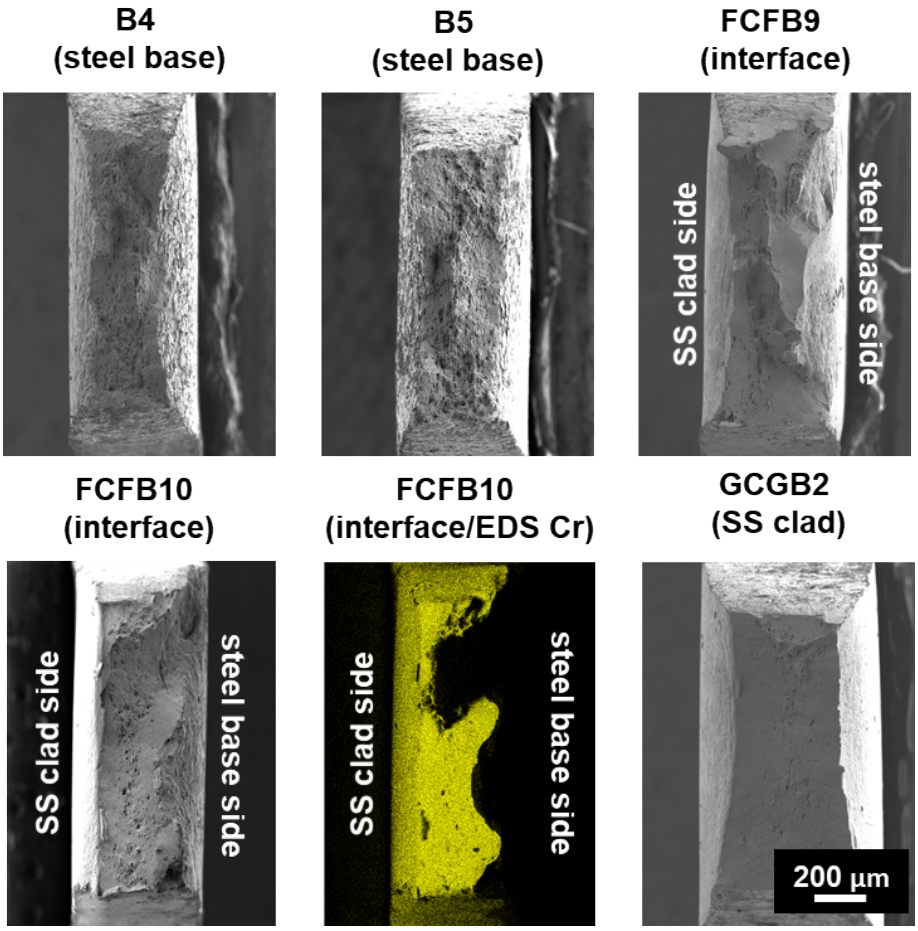

Figure 15. Fracture surfaces of the explosion welded plate corresponding to tensile curves in Figure 15. Energy Dispersive X-ray Spectroscopy (EDS) of Cr for sample FCFB10 highlights the interface between the clad and base sides.

3.2.3 Three-point Bend Properties

Disk specimens were tested by three-point bending until 1 mm of deflection was reached (Figure 16). No specimens fractured during testing and all showed ductile behavior in bending. As can be seen from Figure 17, the bending strength of the stainless steel and carbon steel is two times higher than the uniaxial tensile strength in Figure 14. The samples cut from the interface region were tested both with the stainless steel facing down in the fixture so it would be in tension as well as with the carbon steel side down and in tension in the fixture. The interface region (labeled "composite") had the same strength as the stainless-steel cladding material with either the carbon steel base in tension or stainless steel in tension. Tension is greatest in the center of the bottom surface of the specimen, which allows the stress maximum to be larger due to the reduced amount of material volume. When the carbon steel was in tension, the curves have a feature of a large initial peak stress followed by a smaller peak at larger deflections near 20 % strain. It is not well understood why the stainless steel does not have this feature. Interestingly, when the base metal is in tension, the bending strength is as large as the stainless steel cladding with the exception that it reaches peak stress at lower strain values. When the stainless steel is in tension in the composite, it has the same bend stress curve as the bulk stainless steel specimen. The specimen with a 50 % greater thickness of the stainless steel has a higher peak stress at a higher strain value. It is understood that thicker specimens have a greater volumetric stress that contributes to this artifact in three-point bending and deviates the test from the ideal pure-bending scenario.

Figure 16. Post-bend specimens of the explosion-welded materials and composite.

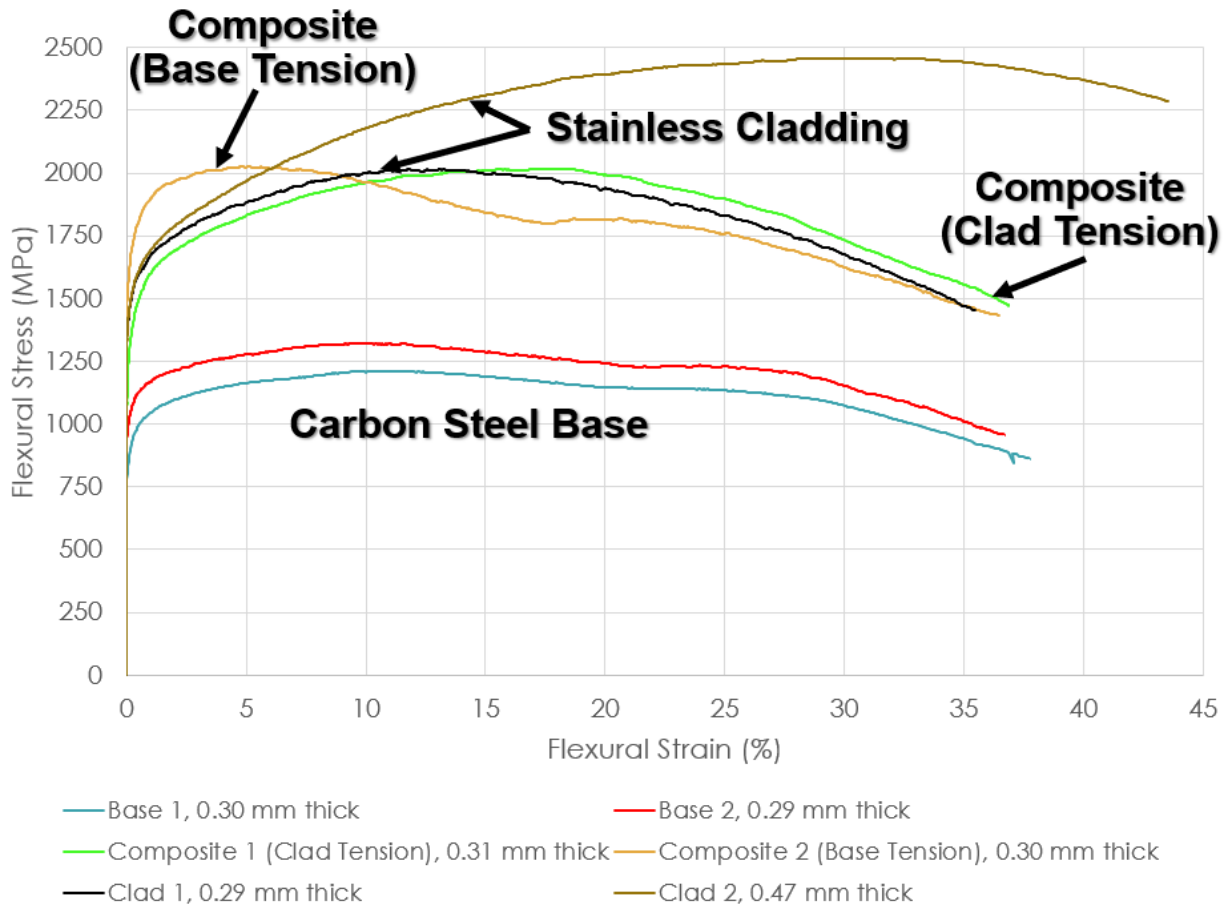

Figure 17. Three-point bend testing stress curves calculated from the geometry and thickness of disk specimens. Specimens were cut in the same method as the tensile tests previously conducted.

3.3 ZIRCALOY-4

3.3.1 Hardness Data

Four welded specimens (unirradiated/irradiated to the highest dose and with/without PWHT) were hardness tested across the entirety of the tensile bar parallel to the tensile axis to capture any differences between the fusion, heat affected, and base metal zones (see Figure 18 and Figure 19). There is no immediately obvious hardness difference between the edges of the samples (presumed base metal – see Figure 2), mid-regions (presumed heat-affected zone), and the center (fusion zone). The lack of a clear base metal region could be attributed to inconsistencies in the distance between center and heat-affected zone/base metal transition on different samples.

Because there was no observable variation between the tab and gauge sections, hardness values collected across the samples are summarized together for each irradiation condition in Figure 20. For unirradiated material, hydrogen charging increases hardness, while welding decreases hardness, regardless of post weld heat treatment or not. Following irradiation to 10^{20} n/cm^2 (E > 0.1 MeV), all samples increase in hardness. At a fluence of 10^{21} n/cm^2, welded and base metal samples show a further increase in hardness, while the hydrogen charged samples do not show such trend due to the large spread in the data.

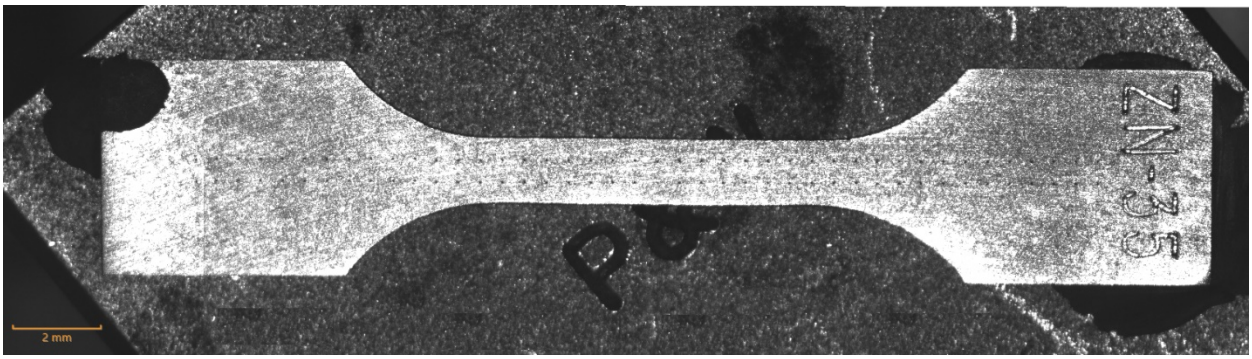

Figure 18. Image of indents going across the gage section of a tensile specimen (ZN-35) in two rows.

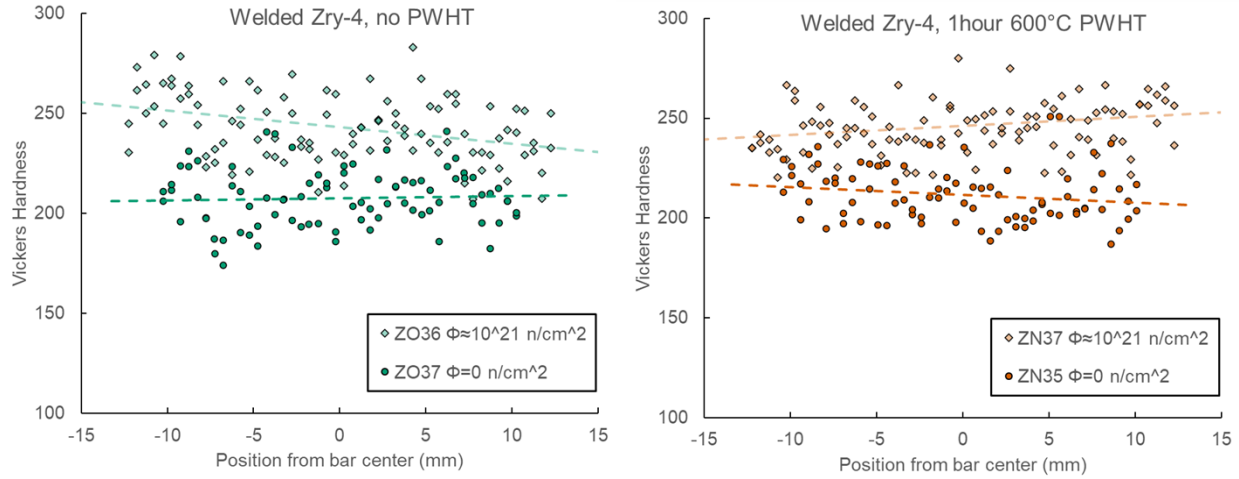

Figure 19. Hardness values measured across the full length of PWHT and no PWHT bars, for both unirradiated and high fluence irradiated conditions. Bar center and weld center are nominally identical; however, local variation may exist. Linear fits for the data are shown as the dashed lines.

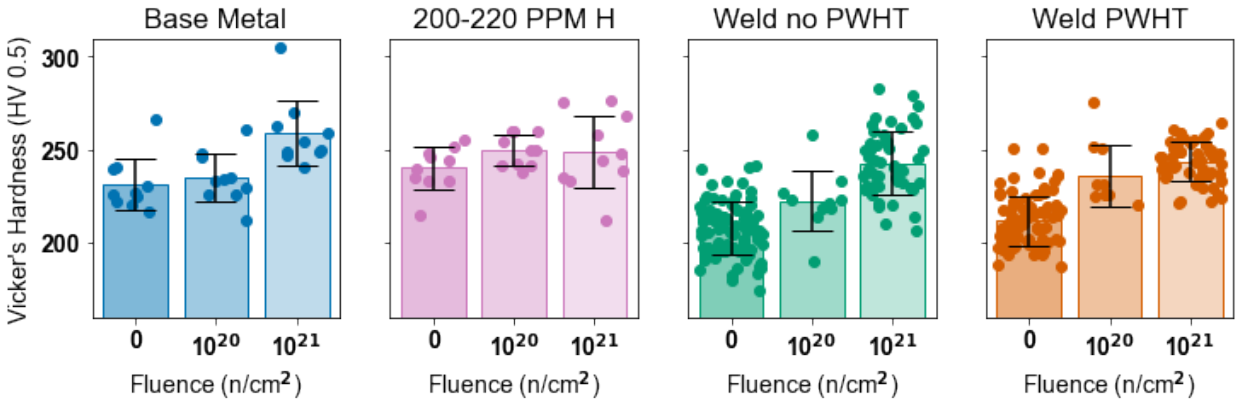

Figure 20. Hardness values for Zry-4 specimens. Dots represent individual data points, bars represent averages, and error bars represent one standard deviation. Fluences are E > 0.1 MeV.

3.3.2 Tensile Properties

Values for yield stress (YS), ultimate tensile stress (UTS), uniform elongation (UE), and total elongation (TE) are shown in Figure 21, with tensile curves for the plastic region shown in Figure 22. Generally, the observed trends are consistent with hardness, where higher hardness is expected to correlate with higher stresses and lower ductility. There is a single exception - welded Zry-4 shows lower hardness when compared to BM, but higher YS and UTS.

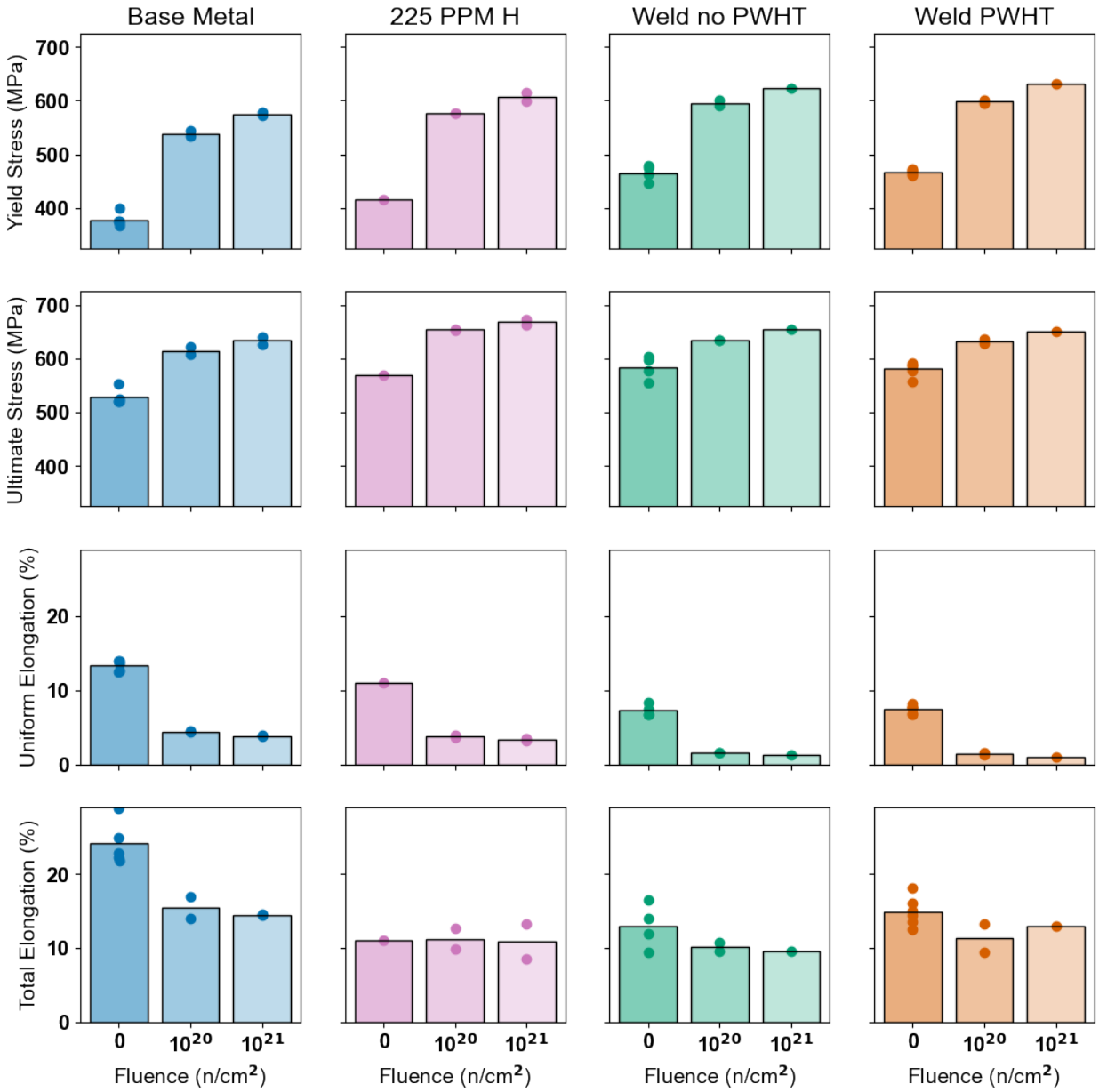

Figure 21. Tensile properties for Zry-4 specimens. Bars represent average values, while dots represent points from individual specimens. Fluences are E > 0.1 MeV

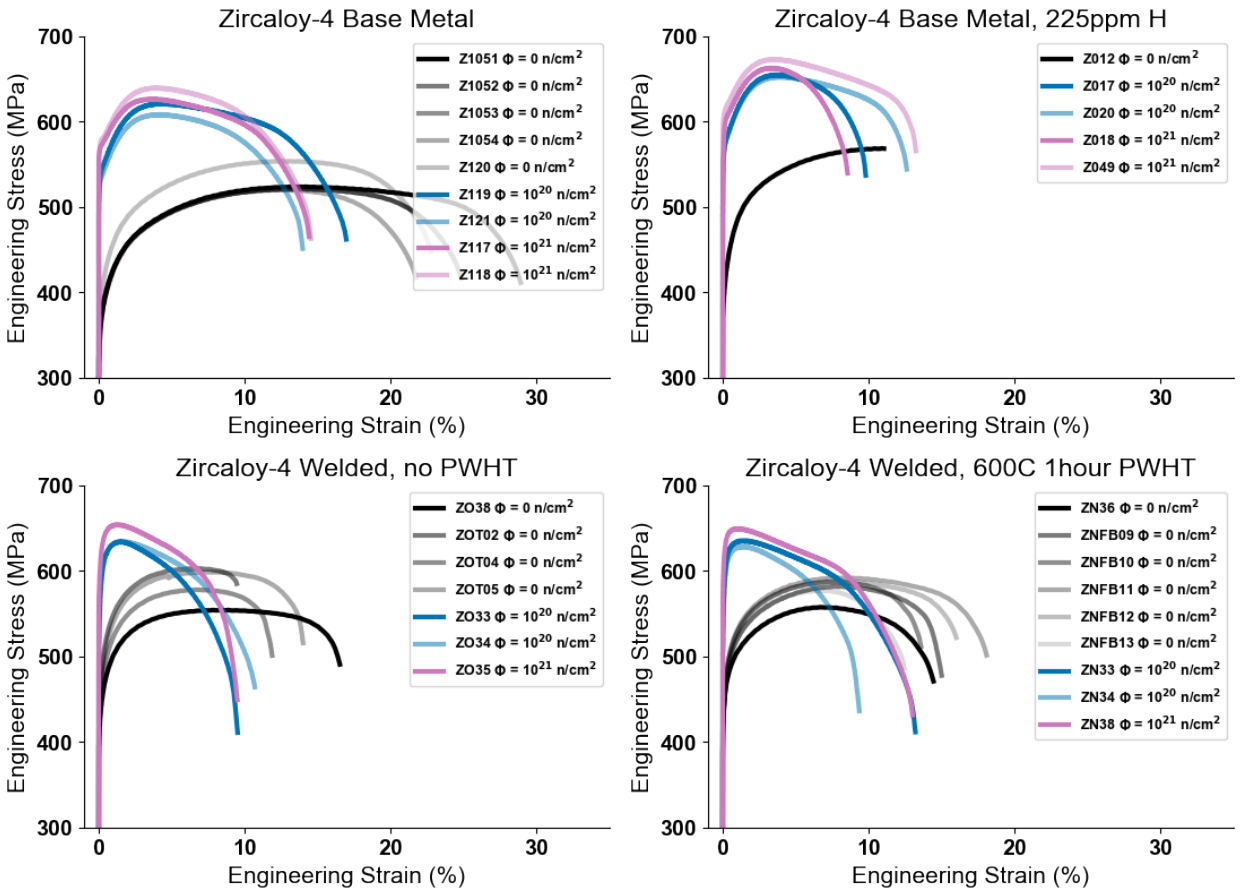

Figure 22. Tensile curves for tested Zry-4 specimens after analysis as described in the Methods section. Data from earlier studies have been added to provide context

Hydriding and welding cause increases to YS/US and decreases to UE/TE at all doses. All specimens show an increase in YS and UTS with increasing doses. UE/TE also decreases with dose, with 2 exceptions: 1) In the hydrided specimens, which have very little change in UE/TE for the irradiated specimens, and average out to the TE as the unirradiated specimen which failed at the UTS. 2) Weld+PWHT specimens show apparently better TE at high dose than low, but it must be noted that there is only a single data point at the highest dose so this trend would need to be confirmed with additional future tests.

Investigating the curves directly, we note that the unirradiated hydrided specimen failed at its UTS, while irradiated specimens exhibit curves more similar to the base metals. Welded specimens all reach their UTS at the beginning of their plastic deformation after irradiation, while base-metal and hydrided specimens have the UTS well beyond their initial plastic deformation.

4. SUMMARY AND FUTURE WORK

The FY21 research for the Shine target solution vessel project focused on:

- Tensile and hardness data collection for irradiated, welded/unwelded Zry-4 (with and without hydrogen charging and PWHT)
- Tensile and hardness data collection for irradiated, unwelded AISI 347.
- 3-point bend, Charpy, and microstructural data collection for explosion-welded AISI 347/ SA-516-70 carbon steel.

Generally, the expected trend of reduced ductility and increasing hardness with increasing dose was observed. The effect prior to a fluence (E > 0.1 MeV) of 10^{20} n/cm^2 tends to be much greater than the effect between 10^{20} and 10^{21} n/cm^2.

For Zry-4, the PWHT samples exhibit the greatest ductility following irradiation. Hydrogen charging and welding with no PWHT degrade the total elongation to a similar amount. On average, however, the gains from PWHT in ductility account for only a few percent compared to the no PWHT case. Welding eliminates the strain hardening capability of the Zry-4 material, while hydrogen-charged samples remain more similar in stress-strain curve shape to the base metal.

For the AISI 347, irradiation produced similar degradation for the 3 suppliers, although Sandmeyer exhibited higher total elongation and lower hardness than the other specimens at intermediate (10^{21} n/cm^2, E > 0.1 MeV) fluence. Charpy-impact testing of unirradiated AISI 347 also shows lower energy for Sandmeyer when compared to all other materials except for the A-orientation of Rolled-alloys. The explosion-welded composite exhibits tensile and 3-point bend properties more similar to the AISI 347 clad than the carbon-steel base.

The remaining 4 capsules of irradiated materials (representing welded AISI 347 and weld/PWHT/hydrogen charged Zry-4) will be tensile and hardness tested in FY22.

REFERENCES

[1] G. R. Piefer, K. M. Pitas, E. N. Van Abel, T. R. Mackie, T. A. Heltemes, R. V. Bynum, & R. F. Radel, (2011, December). Mo-99 production using a subcritical assembly. In Proceedings of the 1st Annual Mo-99 Topical Meeting.

[2] L. M. Garrison, J. Echols, K. Bawane, B. Eckhart, & C. Bryan, (2020) Zircaloy-4 and Stainless Steel 347 Property Data and Microstructures Related to the Structural Material for the Target Solution Vessel and Support Lines of SHINE (ORNL/SPR-2019/1356). Oak Ridge National Lab. (ORNL), Oak Ridge, TN (United States).

[3] L. M. Garrison, J. R. Echols, N. C. Reid, & C. Bryan (2021). Welded and Hydrogen Charged Zircaloy-4 and Welded Stainless Steel 347 Property Data and Microstructures for the Target Solution Vessel and Support Lines of SHINE (No. ORNL/SPR-2020/1879). Oak Ridge National Lab. (ORNL), Oak Ridge, TN (United States).

[4] J. R. Echols, L. M. Garrison, C. Silva, & E. Lindquist (2021). Temperature and time effects of post-weld heat treatments on tensile properties and microstructure of Zircaloy-4. Journal of Nuclear Materials, 551, 152952.

[5] V. S. Tong, T. B. & Britton, (2017). Formation of very large ‘blocky alpha’grains in Zircaloy-4. Acta Materialia, 129, 510-520.

[6] L. M. Garrison, Y. Katoh, N.A.P. Kiran Kumar, Mechanical properties of single-crystal tungsten irradiated in a mixed spectrum fission reactor, Journal of Nuclear Materials 518 (2019) 208-225

[7] N. C. Reid, L. M. Garrison, M. Gussev, and J. P. Allain, "Design and Analysis of an Advanced Three-Point Bend Test Approach for Miniature Irradiated Disk Specimens", Fusion Science and Technology, 77:7-8, 907-914, (2021).

APPENDIX A. SUMMARY TABLES FOR TESTED SPECIMENS

Table 3. Charpy Impact Results

Material Code	Average Impact Energy (J)	Standard Deviation (J)
PA	419	6
PB	411	28
RA	244	24
RB	378	43
SA	282	58
SB	301	36

Table 4. Hardness Results

Material Code	Specimen ID	Approx. Fluence (n/cm^2, E > 0.1MeV)	Average Hardness (HV)	Standard Deviation (HV)
PA	PA02	0	174	8.6
	PA06	1E+20	258	20.1
	PA07	1E+21	265	9.5
PB	PB02	0	179	5.6
	PB04	1E+20	240	7.5
	PB07	1E+21	257	13.8
RA	RA02	0	178	5.7
	RA13	1E+20	244	10.3
	RA09	1E+21	259	15.2
SA	SA02	0	187	5.3
	SA11	1E+20	234	8.1
	SA07	1E+21	261	8.3
Z1	Z120	0	231	13.7
	Z119	1E+20	235	13.0
	Z117	1E+21	259	17.5
Z0	Z12	0	240	11.2
	Z17	1E+20	250	8.3
	Z18	1E+21	249	19.4
ZN	ZN35	0	212	13.6
	ZN33	1E+20	236	16.6
	ZN37	1E+21	245	12.8
ZO	ZO37	0	208	14.2
	ZO34	1E+20	223	16.1
	ZO36	1E+21	243	16.6

Table 5. Tensile Results (AISI-347)

Material Code	Specimen ID	Approx. Fluence (n/cm^2)	Yield Stress (MPa)	Ultimate Tensile Stress (MPa)	Uniform Elongation (%)	Total Elongation (%)
PA	PA01	0	220	723	64	73
	PA02	0	220	724	66	75
	PA03	0	231	670	71	81
	PA04	1E+20	593	754	43	51
	PA06	1E+20	607	760	50	61
	PA07	1E+21	677	780	39	50
	PA08	1E+21	665	790	37	46
	PA09	0	238	722	74	82
PB	PB01	0	220	723	64	73
	PB02	0	220	724	66	75
	PB03	0	231	670	71	81
	PB04	1E+20	549	715	46	55
	PB05	0	237	699	74	82
	PB06	1E+20	565	722	49	56
	PB07	1E+21	643	758	43	51
	PB08	1E+21	614	740	40	48
	PB09	0	237	699	74	82
	PB10	0	246	646	87	97
RA	RA01	0	269	626	83	92
	RA02	0	287	621	71	79
	RA04	0	288	587	77	87
	RA06	0	271	645	79	87
	RA09	1E+21	656	742	47	55
	RA10	0	290	626	74	80
	RA11	1E+21	664	750	43	49
	RA12	1E+20	597	715	44	53
	RA13	1E+20	601	713	42	50
	RA14	0	270	623	80	89
SA	SA01	0	269	626	83	92
	SA02	0	287	621	71	79
	SA03	0	207	631	81	91
	SA04	0	229	635	75	82
	SA05	1E+20	588	733	55	64
	SA07	1E+21	664	759	46	53
	SA08	1E+21	637	786	44	52
	SA11	1E+20	553	765	52	61

Table 6. Tensile Results (Zircaloy-4)

Material Code	Specimen ID	Approx. Fluence (n/cm^2)	Yield Stress (MPa)	Ultimate Tensile Stress (MPa)	Uniform Elongation (%)	Total Elongation (%)
Z0	Z012	0	417	569	11	11
	Z017	1E+20	576	655	4	10
	Z018	1E+21	600	663	3	9
	Z020	1E+20	576	652	4	13
	Z049	1E+21	615	673	3	13
Z1	Z1051	0	371	524	14	29
	Z1052	0	376	521	14	25
	Z1053	0	376	521	14	22
	Z1054	0	368	520	12	22
	Z117	1E+21	573	627	4	14
	Z118	1E+21	578	640	4	15
	Z119	1E+20	544	621	4	17
	Z120	0	400	554	13	23
	Z121	1E+20	534	608	4	14
ZN	ZN33	1E+20	602	635	2	13
	ZN34	1E+20	595	628	1	9
	ZN36	0	461	557	7	14
	ZN38	1E+21	632	649	1	13
	ZNFB09	0	467	582	8	15
	ZNFB10	0	469	587	8	14
	ZNFB11	0	473	592	8	18
	ZNFB12	0	470	588	8	16
	ZNFB13	0	463	577	7	12
ZO	ZO33	1E+20	590	634	2	10
	ZO34	1E+20	600	634	2	11
	ZO35	1E+21	624	654	1	9
	ZO38	0	446	554	8	17
	ZOT02	0	480	603	7	9
	ZOT04	0	463	578	7	12
	ZOT05	0	475	598	8	14